On the Neural Correlates of Motor Imagery With an Extra Virtual Arm

Pinheiro, Daniel Leal; Pollina, Leonardo; Buetler, Karin A.; Marchal-Crespo, Laura; Shokur, Solaiman; Micera, Silvestro

DOI
10.1109/TMRB.2025.3625073

Publication date
2025

Document Version
Final published version

Published in
IEEE Transactions on Medical Robotics and Bionics

On the Neural Correlates of Motor Imagery With an Extra Virtual Arm

Daniel Leal Pinheiro, Leonardo Pollina, Karin A. Buetler, Laura Marchal-Crespo, Solaiman Shokur, and Silvestro Micera

***Abstract*—Motor augmentation (MA) is an emerging field at the intersection of engineering, robotics, and neuroscience, aiming to enhance human capabilities through the integration of extra limbs. This concept leverages the body's physiological redundancies, including those within the nervous system. This study examined motor imagery (MI) involving a virtual extra arm, focusing on differentiating its neural patterns from those of biological limbs. Thirty participants performed unimanual reaching MI tasks before (Pre) and after (Post) a conditioning phase in a virtual environment, during which half of the participants received tactile feedback on the movement of the extra arm. Electroencephalographic (EEG) recordings revealed distinct event-related desynchronization (ERD) in α and β rhythms between the extra and biological limbs. Additionally, a Riemannian decoder successfully classified MI for the left, right, and extra virtual arm, providing further evidence of distinct neural patterns. While the conditioning played a role in the ERD's neural signatures, we did not find the same effects on the decoding. We believe that more complex movements, other sensory encoding modalities, or longer conditioning periods would likely strengthen the connection between tactile feedback and neural control.**

***Index Terms*—Motor augmentation, extra robotic limbs, motor imagery, EEG, brain–machine interfaces.**

I. Introduction

IN MOTOR augmentation (MA), effectively controlling extra degrees of freedom (xDoFs) without compromising the motor function of biological limbs is a critical challenge [1], [2], [3]. Various human-machine interfaces have addressed this issue from various perspectives, focusing on neuroengineering challenges, neuroscientific inquiries, or a combination of both. One promising approach involves harnessing the redundancies present in the musculoskeletal and neural systems to disentangle some of these resources for controlling XDoFs. These redundancies refer to the fact that the human motor system contains more degrees of freedom (e.g., joints, muscles) and control signals (e.g., motor units, cortical activity patterns) than are strictly required for executing most movements.

This strategy could enable the identification of so-called functional task null spaces [1], which are variable spaces, whether kinematic, muscular, or neural, where activity modulation can be utilized to control external interfaces without interfering with other ongoing tasks. Kinematic solutions have leveraged mechanical and robotic designs to achieve seamless integration [4], [5], [6], while others use muscle-based interfaces through electromyographic signals to enable intuitive control [7], [8]. More recently, brain-machine interfaces (BMIs), have gained traction, utilizing neural activity to drive xDOFs [9].

One of the challenges in MA lies in understanding how the brain accommodates and controls these additional effectors while maintaining coordination with biological limbs. Motor imagery (MI) provides a valuable framework to study the neural processes underlying movements and actions, as it engages motor planning and simulation mechanisms without requiring physical execution [10], [11]. MI, motor execution, and action observation are known to share somatotopic correlates in the motor cortex [12]. However, the interpretation and imagery of an extra virtual arm (XVA) introduce unique considerations due to its unconventionality and resemblance to biological limbs. Building on the literature, we question if MI of an XVA will cause the activation of the motor cortex and engage somatotopic brain regions in a manner distinct from biological arms.

This study seeks to advance the exploration of a potential neural null space by examining the neural correlates of MI involving an XVA. The aim is to determine whether neural modulation occurs in motor-related areas and to assess whether the neural patterns of MI of an XVA can be distinguished from those associated with biological limbs. Although existing research has characterized event-related desynchronization (ERD) in alpha (α) and beta (β) rhythms during MI of biological limbs [13], [14], [15], little is known about how these rhythms are modulated when imagining movements of an extra limb [9]. Furthermore, the ability to decode the MI

Received 25 February 2025; revised 8 June 2025 and 27 August 2025; accepted 6 October 2025. Date of publication 23 October 2025; date of current version 2 December 2025. This article was recommended for publication by Associate Editor J. Patton and Editor P. Dario upon evaluation of the reviewers' comments. This work was supported in part by the Bertarelli Foundation; the Swiss National Science Foundation through the National Centre of Competence in Research (NCCR) Robotics Grassroots Project; in part by the European Union's Horizon 2020 Research and Innovation Program through Marie Sklodowska-Curie under Grant 754354; in part by the Horizon Europe Research & Innovation Program (Social and Human Centered XR—SUN project) under Grant 101092612; in part by the #NEXTGENERATIONEU (NGEU); in part by the Ministry of University and Research (MUR), National Recovery and Resilience Plan (NRRP) through the Multiscale Integrated Approach to the study of the Nervous System in Health and Disease (DN. 1553 11.10.2022) under Grant MNESYS PE0000006 and through Tuscany Health Ecosystem (DN. 1553 11.10.2022) under Grant THE IECS00000017; and in part by the Ecole Polytechnique Federale de Lausanne. *(Daniel Leal Pinheiro and Leonardo Pollina are co-first authors.) (Corresponding author: Silvestro Micera.)*

Please see the Acknowledgment section of this article for the author affiliations.

Digital Object Identifier 10.1109/TMRB.2025.3625073

patterns of an extra limb compared to biological ones could provide additional evidence of distinct neural adaptations and support the development of BMIs for MA [1].

Moreover, to further investigate how sensory feedback influences the MI representation of an XVA, we introduced a condition where participants would receive tactile feedback corresponding to the XVA movement during a conditioning phase. This manipulation is motivated by evidence suggesting that sensory feedback, particularly tactile and proprioceptive cues, can enhance motor learning, embodiment, and sensorimotor integration [16], [17]. In the context of MI, where movement execution is absent, the kinesthetic imagery could strengthen the internal representation of the XVA by reinforcing its perceived agency and facilitating its incorporation into the body schema [18].

Thirty participants performed unimanual reaching MI tasks with their left, right, and XVA in a virtual reality (VR) environment. Pre-conditioning (Pre) and post-conditioning (Post) MI assessments were conducted, separated by a conditioning phase where tactile feedback on the XVA was provided to half the participants. Electroencephalography (EEG) data revealed clear ERD patterns in α and β rhythms during MI, with distinct signatures for the XVA compared to biological limbs. In addition to observing these neural modulations, a Riemannian decoding approach was employed to classify MI patterns for the arms. Results demonstrated that decoding performance exceeded significantly theoretical chance levels, with a robust classification of the XVA alongside biological limbs.

This investigation advances the understanding of neural adaptations for MI of extra virtual limbs, providing compelling evidence for the brain's capacity to integrate extra limbs into the motor repertoire. By demonstrating both neural modulation and decoding success, it shows the opportunity for future applications of BMIs in motor augmentation, highlighting the potential for enhanced interaction with additional effectors in real-world scenarios.

II. Methods

The study employed a within-subject design, where all participants performed MI tasks for the left arm, right arm, and the XVA in three phases: pre-conditioning, conditioning, and post-conditioning. The experimental paradigm and the setup are shown in Fig. 1.

A. Participants

Thirty healthy right-handed participants (15 females, mean age = 23.90; SD = 1.84) were recruited for this study. The study was approved by the Commission Cantonale d'éthique de la recherche Genève (BASEC-ID: 2019–02176). All participants provided written informed consent in accordance with the Declaration of Helsinki. Exclusion criteria included a history of neurological disorders or impairments that could affect MI or EEG recordings.

B. Setup and Protocol

Participants were instructed to imagine reaching movements with each arm, following a cue that indicated which arm to imagine moving. The trials were structured with 2s cue, 5s trial, and 2s of intertrial moment (Fig. 1A). The MI tasks were divided into three phases, as illustrated in Fig. 1B:

- *Pre-conditioning phase:* Participants performed MI tasks for the left arm, right arm, and XVA without any additional sensory feedback. During this phase, they watched a video with the trial-corresponding arm moving in the way they should imagine (Fig. 1C). The purpose of this phase was to assess baseline neural activity related to the MI of each limb. The XVA was designed with a chirality-neutral configuration to avoid biasing participants toward imagining movement of either the right or left arm (Fig. 1C).
- *Conditioning phase:* Participants were immersed in a VR environment, where the imagined movements of each arm were visually represented in real-time with an avatar from a first-person perspective (Fig. 1D). In addition, a subgroup of participants (N = 15) received tactile feedback corresponding to their imagined movements. The tactile feedback (Fig. 1E) consisted of pressure delivered to the chest of the participant through a servo motor, that would linearly increase the intensity according to how far the XVA was in relation to the starting position. This phase aimed to reinforce the neural associations between MI and external feedback for each limb.
- *Post-conditioning phase:* Following the conditioning phase, participants once again performed the MI tasks for each limb, as in the pre-conditioning. This phase was designed to assess changes in neural patterns after conditioning and whether the tactile feedback enhanced the neural differentiation between limbs during MI tasks.

For the MI task, participants were instructed to mentally simulate the movement of the cued arm, imagining the execution of the displayed movement as presented in the video or VR, without any muscle engagement. For the extra virtual arm, they performed the imagery process solely based on the concept of controlling a limb in that disposition, relying entirely on their internal representation of such movement. Each arm underwent 20 trials per task.

C. EEG Recordings

Continuous EEG (Fig. 1F) was recorded throughout all phases using a 61-channel system with electrodes positioned according to the 10-10 international system. EEG signals were sampled at 2000 Hz and band-pass filtered between 1.5 and 45 Hz. Impedance levels were maintained below 20 kΩ for all electrodes to ensure optimal signal quality. Participants were instructed to remain still during the tasks to minimize movement-related artifacts.

D. Data Preprocessing and Spectral Analysis

We focused on the alpha (8-12 Hz) and β (12-30 Hz) frequency bands to explore the neural dynamics associated with MI, as these rhythms are strongly linked to motor-related neural activity [19]. The analysis was restricted to central EEG channels primarily closer to the sensorimotor region (Fig. 1F).

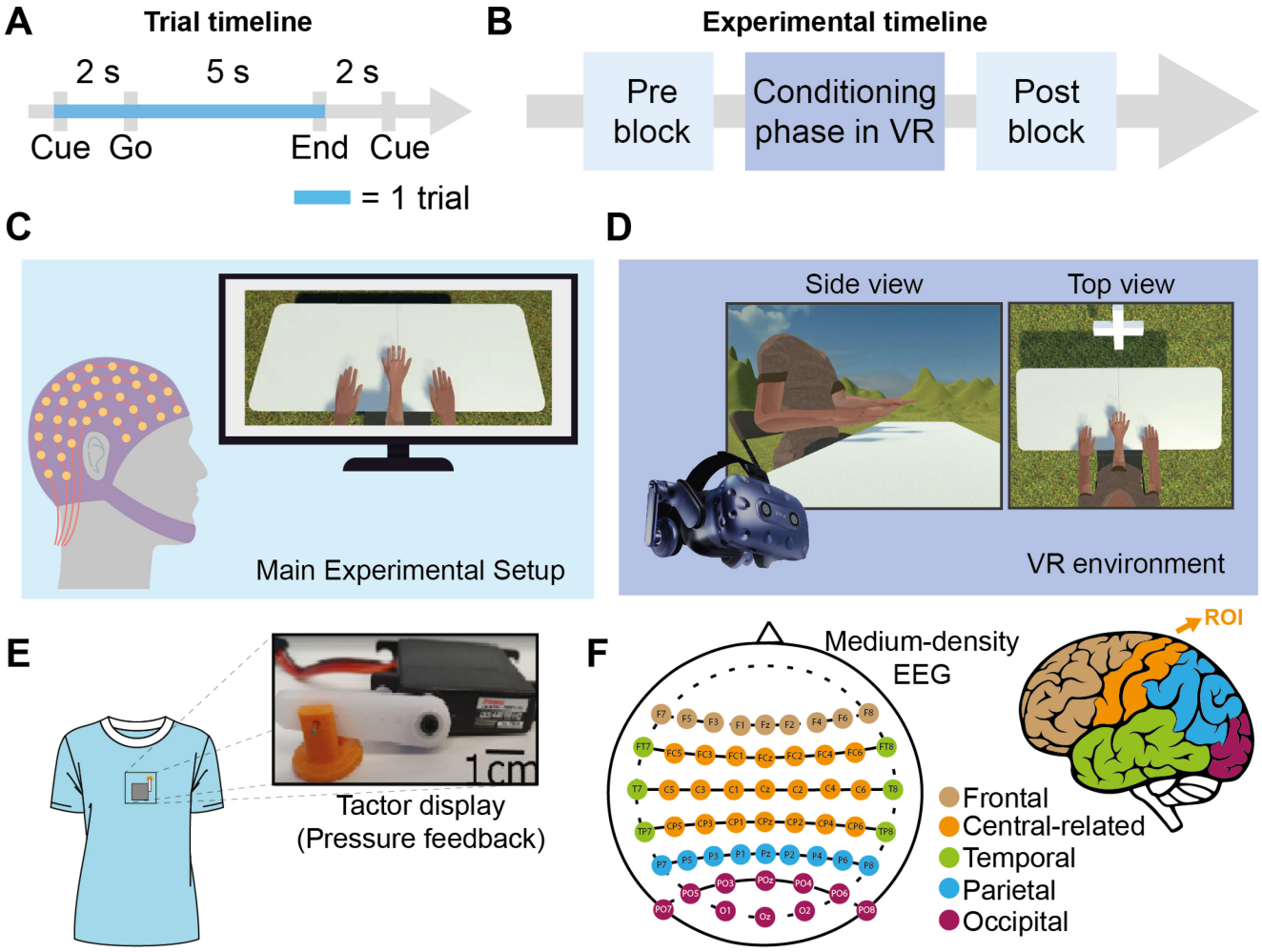

Fig. 1. Experimental paradigm and setup. **A** The trial structure followed a standard MI paradigm. A cue indicating the movement to be imagined was presented, followed by a 2-s delay before a go signal, which marked the start of the MI phase. The MI phase lasted 5 s and was followed by a 2-s intertrial interval. **B** The experimental paradigm was divided into three consecutive phases: the first and third one consisted of the actual MI tasks, while the second one consisted of a conditioning phase in Virtual Reality. **C** The main setup of the experiment included the EEG cap that was worn throughout the whole length of the experiment together with a screen showing the reaching movement to be imagined with each arm. **D** During the conditioning phase, the participant wore the Virtual Reality (VR) headset (Vive Pro Eye HMD; HTC Corporation, Taiwan). The VR environment consisted of an avatar with a third arm coming out from the middle of the chest and sitting in front of a table. The arms would be positioned in an initial resting phase and would move automatically towards targets appearing randomly for each one of the arms (unimanual reaching), similarly to the environment used in [4]. **E** In the Tactile (T) group, a tactor display applying pressure during the movement of extra virtual arm (XVA) was positioned in the middle of the chest of the participant, which corresponds to the position of the XVA in the VR environment. **F** We used a 61-channels EEG cap, but we defined our region of interest (ROI, in orange) as the central area containing frontocentral, central and centroparietal areas as these ones span the main motor regions.

Event-related spectral perturbations (ERSP) maps were computed using continuous wavelet transforms (CWT) with a Morlet wavelet to derive time-resolved power spectral representations of the EEG signals. Each trial's power map was baseline-normalized relative to the –1 to 0 second window preceding the Go signal. This normalization was applied across all frequency bins and time points, yielding ERSP maps expressed in dB units.

To explore the spatial dynamics of sensorimotor engagement during MI, we computed time-resolved topographical maps of combined α and β bands power (Fig. 2). EEG signals were segmented into epochs of 1s from -2 s to 7 s relative to the imagery cue (0 s), encompassing the preparatory phase (-2 to 0 s), the MI phase (0 to 5 s), and the inter-trial/post-imagery phase (5 to 7 s).

For each subject and condition, the median ERSP map was then computed across all trials at each channel, reducing the influence of outlier trials and capturing a robust representation of condition-specific activity, as shown in Fig. 3.

To quantify synchronization or desynchronization levels for statistical analysis, we extracted the mean power within the α and β bands and within the defined temporal intervals: the motor preparation period (-2 to 0 s) and the imagery period (0 to 5 s). These band- and time-averaged power values were computed at the subject level and then used as dependent variables in the mixed-effects statistical models.

Specifically, we evaluated the influence of the imagined limb (left, right, or extra), the task phase (motor preparation vs. MI), the conditioning group (tactile vs. non-tactile feedback), and the session (pre-conditioning vs. post-conditioning). This analysis aimed to determine how these factors individually and interactively affected neural desynchronization patterns, providing insights into the underlying dynamics of MI and its modulation by external feedback and training.

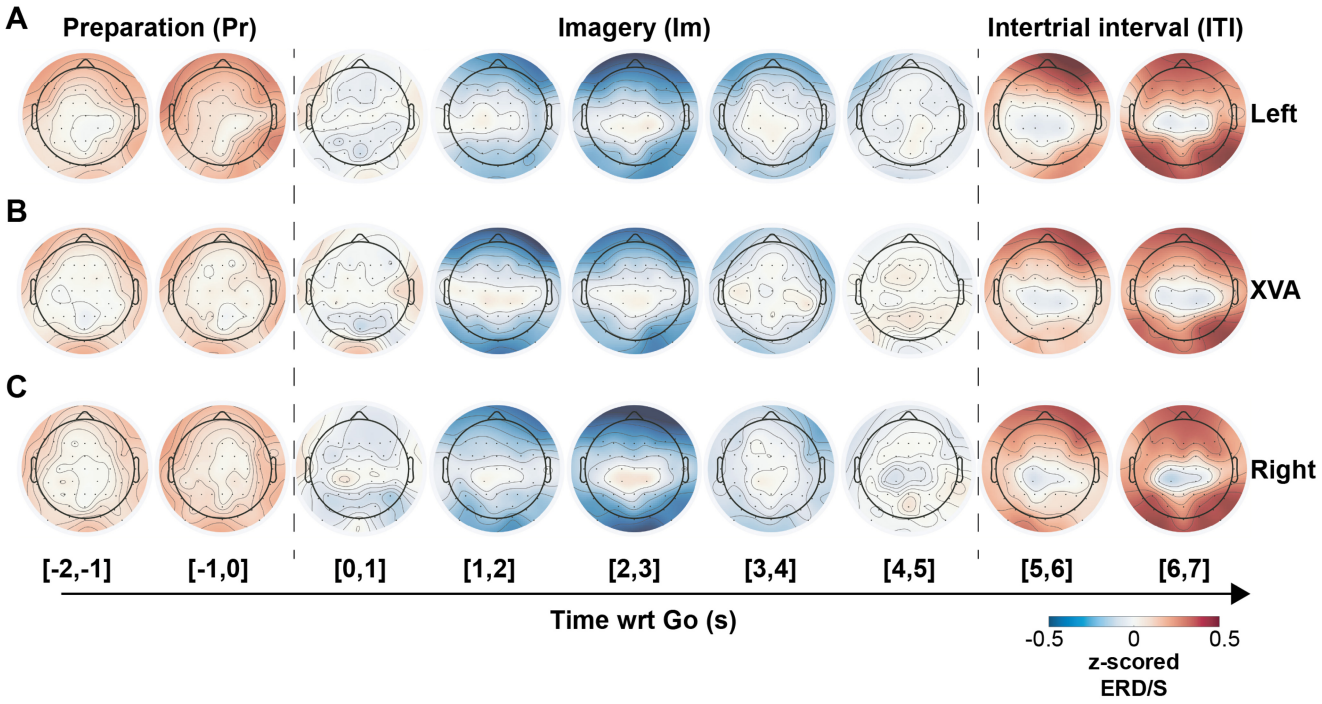

Fig. 2. Time-resolved topographical distribution of ERD/S patterns during MI tasks for each arm condition. A. Left arm, B. XVA, C. Right arm. Each subplot displays a sequence of topographical maps showing combined α and β power dynamics over time, computed using a -2 to 7 s epoch relative to imagery onset (Go signal, 0 s). The maps illustrate cortical activity during three key periods: the preparatory/cue period (-2 to 0 s), the MI period (0 to 5 s), and the inter-trial/post-imagery period (5 to 7 s). Desynchronization is most prominent over central sensorimotor regions, with biological arms showing patterns consistent with motor engagement. The XVA condition exhibits a more bilaterally distributed and diffuse modulation, likely reflecting the integration of a novel effector without a predefined somatotopic representation.

For the comparisons across limbs, ERD/S values were calculated by averaging power changes across the predefined region of interest (ROI), Fig. 1F, covering all central-related electrodes. This included frontocentral, central, and centroparietal channels, thereby encompassing the main motor areas without lateralization bias. This approach was chosen to provide a comprehensive estimate of motor-related desynchronization for each imagined limb.

This approach enabled a detailed examination of ERD patterns in the α and β bands, which reflect cortical activation during MI tasks. The focus on central EEG channels ensured that the analysis captured motor-related neural activity with high specificity.

E. Decoding of Motor Imagery

To decode the movement performed during the MI tasks of the experiment, that is the reaching movement with the right, the left, or the extra arm, we used a Riemannian geometry-based approach [20], [21], [22] by using the Python machine learning package `PyRiemann` [23]. This method leverages the covariance structure of the neural data, mapping each trial to a symmetric positive-definite (SPD) matrix that encodes inter-channel dependencies within the neural signals. This method contains two direct advantages: it does not require particular spatial filtering methods, since the covariance matrices encode it directly, and leverages directly the temporal information of the signal.

In particular, we used the Minimum Distance to Mean (MDM) classifier, which calculates class centroids as the Riemannian mean of covariance matrices for each class and assigns a class to new trials based on their Riemannian distance to these centroids [20]. We independently trained separate classifiers for each subject and for the two temporal conditions (Pre and Post). The effect of tactile stimulation was assessed by aggregating individual subject decoding results within the T and NT groups. To assess the overall content of the information during the whole trial, 5 seconds of broadband pass-filtered EEG signals following the Go signal were used to train the classifiers and compute the covariance matrices. We cross-validated our results using 10 stratified folds, ensuring that both the training (54 trials) and test (6 trials) sets were evenly balanced across arm labels, given the initial 20 trials per arm. As an evaluation metric, we used balanced accuracy (BA), which is defined as the arithmetic average of the recall for each class:

$$Rec_{class_j} = \frac{TP_j}{TP_j + FN_j} \quad for\ j \in 1, \ldots, J \tag{1}$$

$$Balanced\ Accuracy\ (BA) = \frac{1}{J} \sum_{j=1}^{j=J} Rec_{class_j} \tag{2}$$

being TP_j the true positive of the j^{th} class, FN_j the false negative of the j^{th} class, FP_j the false positive of the j^{th} class, and J the total number of classes.

F. Lateralization Effect on Decoding Performance

To identify the most informative channels for classification, we conducted a removal-based analysis inspired by [24]. Given

the specific regions of interest and the inherent redundancy of covariance matrices, which tend to be robust to the removal of individual channels, we focused on the role of lateralized neural modulation during the MI process. For this analysis, we examined the Pre and Post conditions separately but combined the T and NT groups, based on the absence of significant group differences identified in the decoding analysis (Fig. 4B). Specifically, for each participant, we repeated the decoding procedure described in Section II-E, but removed either all left-side channels (FC1, FC3, FC5, C1, C3, C5, CP1, CP3, CP5) or all right-side channels (FC2, FC4, FC6, C2, C4, C6, CP2, CP4, CP6). We then computed, for each subject, the percentage decrease in decoding accuracy relative to the original accuracy using all channels, $D_{R/L\_\%}$, defined as:

$$D_{R/L\_\%} = 100 * \frac{Acc_{All\_channels} - Acc_{W/o\_L/R}}{Acc_{All\_channels}} \quad (3)$$

where, $Acc_{All\_channels}$ represents the accuracy computed with all channels, and $Acc_{W/o\_L/R}$ is the accuracy computed without the left (L) or right (R) channels. To understand which classes were affected by the lateralization analysis, we computed the median absolute change confusion matrices. These correspond to the median across participants of the absolute change in prediction probability between the original decoding confusion matrix (i.e., the one obtained using all channels of interest) and the confusion matrix obtained after selecting only one-side channels. We used the absolute change rather than the relative change to avoid divisions by zero, which are common when working with confusion matrices.

G. Decoding Through Time

To gain insight into the neural dynamics underlying the MI process and to find at what time points during the trial the three classes were the most distinguishable, we performed a decoding analysis focusing on individual time windows that progressed throughout the trial. Specifically, each trial consisted of 9 seconds of neural data, divided into three phases: 2 seconds of intertrial, 2 seconds of preparation following the Cue signal, and 5 seconds of MI. Using the methodology described in Section II-E, we segmented the signal into overlapping time windows of 500 ms, with a shifting step of 100 ms. Classifiers were trained and tested separately for each time window.

To complement this analysis and assess the generalization capabilities of our decoders from a more translational perspective, we conducted an analysis inspired by a pseudo-online decoding approach [25]. Specifically, we performed a 10-fold stratified cross-validation in which the classifier was trained using the entire 5-second MI interval. The trained model was then tested on the held-out data using sliding time windows of 500 ms, advanced in 100 ms steps. This setup allows us to evaluate how well a classifier, trained on robust covariance estimates from long time segments, generalizes to shorter, unseen windows. Importantly, the 100 ms step size is consistent with a potential update frequency for practical online BMIs. It is worth noting that in this analysis, EEG signals were initially broadband band-pass filtered before classification. In a real-time online scenario, however, preprocessing steps would need to be adapted and implemented in real time as well.

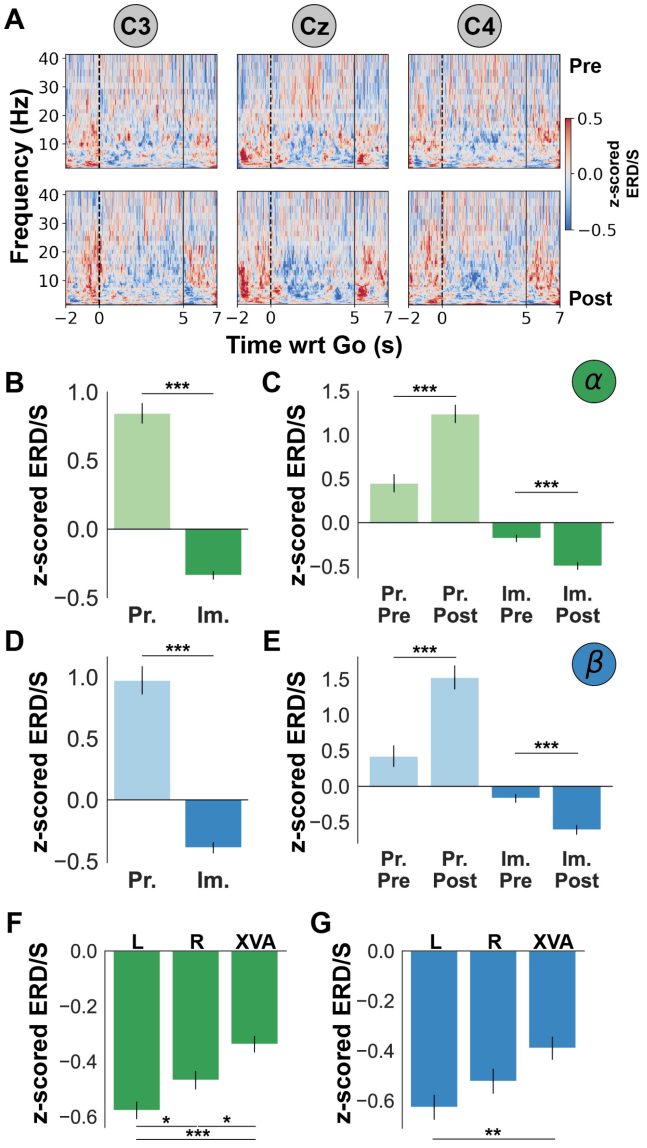

Fig. 3. Neural correlates related to XVA's motor imagery. **A** Grand-average ERSP maps for motor imagery of the XVA (Cz), left arm (C4), and right arm (C3), showing power modulation over time and frequency. The extended time window includes the preparation (−2 to 0 s), imagery (0 to 5 s), and post-imagery intertrial period (5 to 7 s), enabling observation of α and β modulation throughout the process. The baseline was set from –1 to 0 s relative to the Go signal B Overall level of ERD/S in the α frequency band for both preparatory (Pr., i.e. [-2, 0] s) and imaginary (Im., i.e. [0,5 s]) activity. C ERD/S levels divided for moment (Pr. and Im.) and condition (Pre and Post). D and E are the same as B and C, respectively, but for the β frequency band. Overall ERD/S levels during the Imaginary activity when comparing the movements involving the biological limbs and the XVA for F α, and G β bands. * indicates statistical significance at p< 0.05, ** at p< 0.01,and *** at p< 0.001.

H. Statistical Analysis

A linear mixed-effects model was fit to the power values derived from the ERSP maps. The fixed effects included Arm (left, right, or extra), Task (pre-conditioning or post-conditioning), Group (tactile or non-tactile feedback), and their interactions. The Subject was modeled as a random intercept to account for inter-subject variability. The model aimed to test for the main effects and interactions of these factors on desynchronization power. Separate analyzes were performed for α and β rhythms. Additionally, a focused analysis was conducted on the neural activity associated with the XVA. For

this subset of the data, the model included Moment (motor preparation vs. MI), Task, and Group as fixed effects, with Subject as a random intercept. This analysis provided a finer evaluation of the neural dynamics associated with the XVA.

ANOVA was performed on each mixed-effects model to examine the significance of the fixed effects and their interactions. To ensure rigorous control of type I error due to multiple comparisons, significant interactions were further assessed using post hoc pairwise comparisons with Bonferroni correction. Pairwise post-hoc comparisons were also followed by the computation of Cohen's d effect sizes to assess the magnitude of observed differences.

Regarding the decoding analysis, the overall decoding performance was measured as the average balanced accuracy across participants. This group-level accuracy was considered significant if it exceeded the average 95^{th} percentile of the chance accuracy distribution, determined through 1000 iterations of label shuffling per subject (permutation test). For the decoding evolving over time, the same method was used independently for each time window.

To assess the effects on decoding performance when using only channels located on one side of the brain, we applied a one-sample Wilcoxon signed-rank test.

Whenever necessary, distributions were tested for normality prior to the use of parametric tests via the Shapiro-Wilk test with $\alpha = 0.01$.

III. Results

A. Neural Modulation During MI Process

The analysis of neural modulation during the MI process revealed significant changes in α and β rhythm power, as observed by the topographical and the grand average spectral maps in Figs. 2 and 3A. These changes highlight the modulation of neural activity during the transition from preparation to motor imagery, emphasizing the dynamic nature of rhythmic activity during MI tasks. Although we conducted a mixed-effects analysis including all factors involved in the experiment, the following will focus on those that showed a significant effect.

With the topographical maps, Fig. 2, we observed desynchronization over the ROI region, consistent with motor-related cortical activity. For the biological arms, desynchronization shows a trend of contralateral response. In contrast, the XVA condition elicited a more spatially diffuse and bilateral pattern across central electrodes, with less focal modulation. During the inter-trial period (5–7 s with respect to Go signal), we also observed a rebound of β activity, particularly in lower β frequencies, consistent with post-imagery re-synchronization of motor rhythms (Fig. 3A). These spatial features complement the spectral findings, highlighting differences in how biological and virtual limbs engage cortical networks during motor imagery.

Concerning the analysis over the XVA only, the α rhythm showed a significant difference in power between the preparation and motor imagery phases ($F = 17.16$, $p < 0.001$, DF $= 1672$), Fig. 3B. This result shows modulation of α power during the MI process, demonstrating the neural engagement associated with the XVA. Furthermore, the interaction between moment and task for the α rhythm was also significant ($F = 14.74$, $p < 0.001$, DF $= 1672$). Posthoc comparisons revealed significant differences across α power during MI post-training compared to preparation post-training ($p < 0.001$), Cohen's d indexes between preparation and imagery for the Pre and Post conditions are 1.08 and 0.39, respectively, (Fig. 3C).

When looking at the β rhythm during the XVA MI, we found a significant difference in power between the preparation and motor imagery phases ($F = 4.13$, $p < 0.05$, DF $= 1672$), further corroborating the presence of strong modulation of neural activity during MI (Fig. 3D). The interaction between moment and task for the β rhythm was also significant ($F = 19.18$, $p < 0.001$, DF $= 1672$). Posthoc comparisons revealed significant differences between imagery and preparation phases, with β power decreasing notably during motor imagery post-training compared to preparation post-training ($p < 0.001$), and similar reductions observed pre-training ($p < 0.01$), Fig. 3E. Cohen's d indexes between preparation and imagery for the Pre and Post conditions are 0.82 and 0.43, respectively.

Comparisons across the three arms (left, right, and XVA) revealed significant differences in both α and β rhythms. For the α rhythm, a main effect of the arm was observed ($F = 21.72$, $p < 0.001$, DF $= 2508$), Fig. 3F. Posthoc comparisons showed significant differences between the left arm and the XVA ($p < 0.001$, Cohen's $d = 0.27$) as well as between the right arm and the XVA ($p < 0.05$, Cohen's $d = 0.14$) and left and right ($p < 0.05$, Cohen's $d = 0.12$). For the β rhythm, Fig. 3G, the main effect of the arm was also significant ($F = 3.08$, $p < 0.05$), with posthoc comparisons indicating significant differences between the left arm and the XVA ($p < 0.01$, Cohen's $d = 0.17$). These results point to distinct neural signatures for the XVA compared to the biological arms, which highlight the potential for effectively decoding neural activity associated with the control of an extra limb.

Finally, in addition to the preparation and imagery phases, the ERSP maps include a post-imagery intertrial period (5–7 s with respect to Go signal) to enable visual inspection of post-movement neural dynamics. Across all conditions, a clear increase in β power, especially in the lower β band, is observed following the end of thwee motor imagery phase (Fig. 3A). This phenomenon, commonly referred to as β rebound, has been associated with the inhibition of motor areas and a return to an idling state of the sensorimotor system following motor execution or imagery [26], [27], [28]. The presence of this rebound effect, even in the absence of overt movement, further supports the engagement of sensorimotor networks during imagined movements, including for the control of novel effectors such as the XVA.

B. Decoding of MI

After having observed changes in neural dynamics during the MI of the XVA, we tested whether the arm involved in MI could be classified using a decoding analysis. For this, we employed a Riemannian-based classifier, which computes the

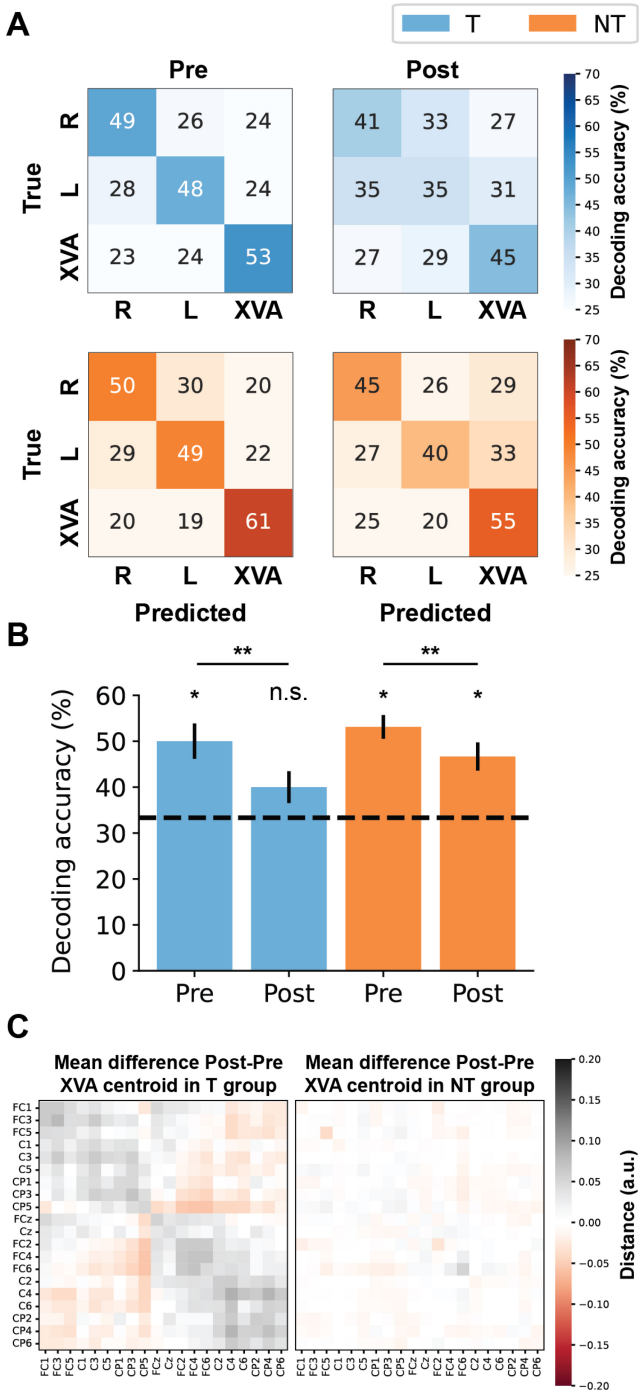

Fig. 4. Three-classes decoding performances during motor imagery. **A** Average normalized confusion matrices across subjects for both groups (T and NT) and tasks (Pre and Post). **B** Average decoding performances across participants for both groups and Pre and Post tasks. The dashed line represents the theoretical chance level. Error bars represent the standard error of the mean across participants. * indicates statistical significance at $p < 0.05$, ** at $p < 0.01$. **C** Mean across participants of the differences between the normalized XVA centroids in the Post and Pre tasks, both for the T (left) and NT (right) group. The centroid is here the representative covariance matrix characterizing the XVA class during the Riemannian decoding.

covariance matrices across the considered channels for each trial. A general centroid covariance matrix is then determined for each class, and new trials are assigned a class based on their minimum distance to these centroids. The decoding was performed using broadband EEG signals in the 1.5–45 Hz range.

Our results showed significant decoding accuracy ($p < 0.05$, permutation test) for both Non-Tactile (NT) and Tactile (T) groups in the Pre condition. However, in the Post condition, significant decoding was observed only for the NT group. Notably, the XVA class was the most accurately decoded in all cases, as indicated by the confusion matrices in Fig. 4A. Specifically, overall balanced decoding accuracies were 50 ± 4% (mean ± SEM across participants) for the T-Pre group, 53 ± 3% for the NT-Pre group, 40 ± 3% for the T-Post group, 47 ± 3% for the NT-Post group, as shown in Fig. 4B.

A mixed-effects ANOVA comparing these four groups revealed a significant effect of the task, with Pre condition accuracies being higher than Post condition accuracies ($F = 12.24$, $p < 0.01$). To further examine how the neural representation of the XVA class changed between the Pre and Post tasks in the T and NT groups, we computed the difference between the normalized centroids of the XVA class for each participant and averaged these differences across participants. Fig. 4C illustrates these mean differences, illustrating how the covariance matrix representing the XVA class remained more stable in the NT group compared to the T group.

We also aimed to determine whether certain channels contributed more than others to the classification performance. To this end, we conducted a removal-based analysis, in which decoding accuracy was recomputed after excluding either the left-side or right-side channels. This analysis was performed separately for the Pre and Post conditions. In the Pre condition (Fig. 5A), removing right-side channels resulted in a significant decrease in balanced accuracy of 10% ± 9% (median ± median absolute deviation) compared to the original performance using all channels ($p<0.01$, one-sample Wilcoxon signed-rank test, Bonferroni corrected). In contrast, removing left-side channels did not lead to a significant drop in performance (3% ± 8%). A similar trend was observed in the Post condition, although the effect did not reach statistical significance (Fig. 5B). In Fig. 5C, we report the median absolute change across participants in the prediction probabilities for the confusion matrices of the PRE condition, providing insights into how classification patterns changed when removing left-side or right-side channels. When left-side channels were removed, we observed an overall decrease in the correct prediction of Right Arm (R) MI trials (5% decrease), accompanied by an increase in misclassification of R MI trials as XVA MI trials (5% increase). Interestingly, the removal of left-side channels also led to an increase in the correct prediction of Left Arm (L) MI trials (5% increase). Conversely, when right-side channels were removed, the correct decoding of L MI and XVA MI trials decreased (8% and 5% decrease, respectively), while the likelihood of misclassifying L MI and XVA MI trials as R MI trials slightly increased (2% increase for each).

C. Decoding of MI Through Time

To gain some insights into the temporal separability of different imagined movements, we conducted a decoding

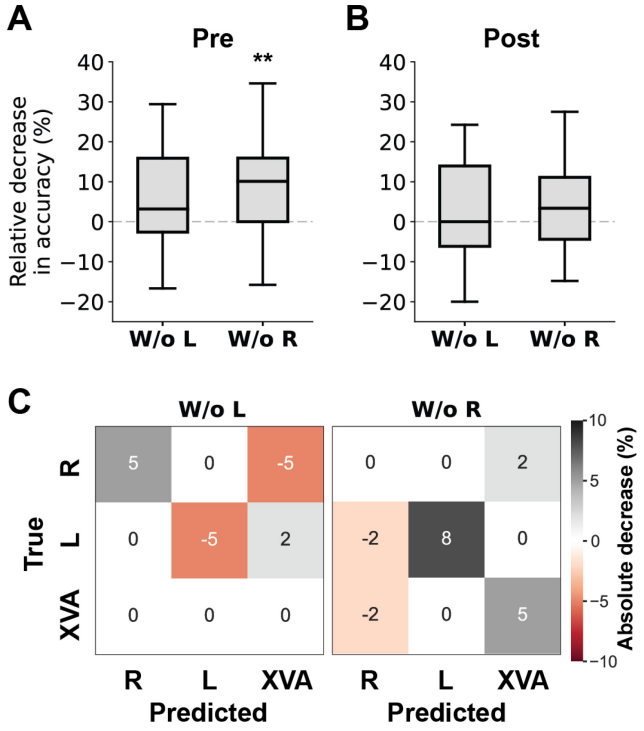

Fig. 5. Effect of lateralized channel removal on decoding performance for **A** the Pre, and **B** the Post condition. Boxplots show data from 30 participants, with groups T and NT combined for this analysis. Values represent the relative decrease in accuracy when removing channels from one side of the brain (L = left, R = right). **C** Absolute change in prediction probabilities of the confusion matrices for the PRE condition when removing the left channels (W/o L, on the left) or the right channel (W/o R, on the right). "W/o" stands for "without". ** denote statistically significant differences from zero with $p < 0.01$ (one-sample Wilcoxon signed-rank test, Bonferroni corrected for multiple comparisons).

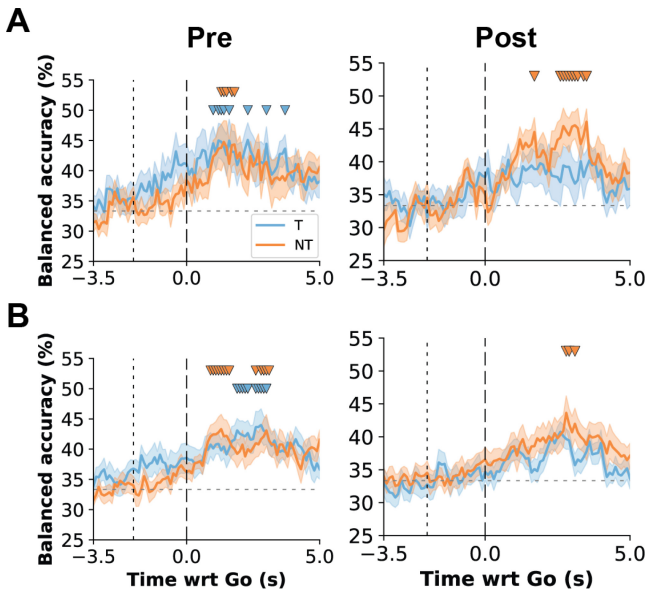

Fig. 6. Time-resolved decoding accuracy for both the Pre (on the left) and Post (on the right) conditions. **A** Analysis performed by training and test the classifier for every time window independently. **B** Analysis performed by training a single classifier over the whole duration of motor imagery and testing it on sequential time windows from the test set. For both panels, the thick line represents the average accuracy across participants, while the colored faded area is the standard error of the mean. The vertical dotted line and dashed line correspond to the Cue and Go signals, respectively. The horizontal dotted line is the theoretical chance level. On the time axis, the time points reported are the last time point of every time window with respect to (wrt) the Go signal. Triangles indicate when the accuracy was higher than the 95^{th} percentile of the chance distribution obtained via labels shuffling.

analysis by training and testing our Riemannian classifier on consecutive overlapping time windows of 500 ms with a 100 ms step. The analysis began during the intertrial period, serving as a negative control that produced chance-level decoding accuracies as expected.

The results aligned with the patterns described in Section III-B, showing significant decoding accuracies for both the T and NT groups in the Pre condition (Fig. 6A), and significant accuracies exclusively for the NT group in the Post condition (Fig. 6B).

In the Pre condition, the window of significant decoding was predominantly between 1 and 2.3 seconds after the Go signal for both groups. Notably, this window shifted for the NT group in the Post condition, where significant decoding occurred primarily between 2.5 and 3.5 seconds after the Go signal.

To further validate our approach and advance towards generalization and translational applications, we conducted a time-resolved decoding analysis simulating a pseudo-online decoder. A single classifier was trained on the entire duration of MI data from the training set and then applied to consecutive time windows in the test set. The results supported the patterns observed in earlier analyzes: both the T and NT groups showed significant decoding performance between 1 and 3 seconds after the Go signal during the Pre condition (Fig. 6B). In contrast, only the NT group exhibited significant performance in the Post condition, around 3 seconds after the Go signal, consistent with the prominent peak shown in Fig. 6A.

IV. Discussion

The main goal of this study was to investigate the neural correlates of MI with XVA for use in MA paradigms, with a particular focus on how the brain allocates resources to control xDOFs through the MI of an additional limb. Our results provide insights into three key aspects: (1) the distinct neural correlates of MI of the biological limbs and the XVA; (2) the role of conditioning, particularly using VR, in enhancing neural engagement for MI tasks; and (3) the impact of tactile feedback in the neural representation of the XVA.

A. Motor Imagery Signatures Across Arms

Our results revealed significant MI neural correlates for all three arms, including the XVA, which is in agreement with the established literature on tool and limb imagery [18], [29], [30], [31]. Previous studies have shown that imagined actions with external tools or limbs elicit neural activity that resembles the brain's motor command patterns for biological limbs [12]. However, our findings take a step further by showing that the neural signatures associated with the XVA diverge from those of the biological arms, particularly focusing on the α and β rhythms. This divergence is intriguing, as the XVA is not a

natural limb that is imagined in an unconventional position. Unlike familiar tools or prosthetics, the XVA's positioning and control interface challenge traditional body schemas, which could lead to more distinct neural activity patterns. These results point towards the brain's capacity to adapt and encode novel motor representations, enabling the integration of non-biological appendages, even when their location and function are unconventional. The presence of such differential signatures suggests that our neural processing of the XVA points to the flexibility of the brain's motor systems in accommodating new and unconventional tools, a result also supported by [9], where authors explored MI correlates of an extra thumb.

To investigate the spatial dynamics of sensorimotor engagement during MI, we visualized α and β ERD/S topographies across conditions, as presented in Fig. 2. Across all arms, we observed robust desynchronization over central regions; however, for the XVA, this pattern was more bilaterally distributed. Such non-lateralized activity is consistent with prior studies reporting bilateral activation during complex or full-limb MI [32], and with the more spatially distributed cortical responses observed during visual-motor or less embodied imagery strategies [33]. These findings support the idea that controlling a novel effector like the XVA relies on broader sensorimotor and associative cortical networks, possibly reflecting the additional demands of integrating an unfamiliar limb into one's body schema.

Concerning the conditioning phase, our results also suggest that VR plays a role in modulating neural engagement during MI tasks. The ERDS analysis revealed enhanced α and β power modulation in the post-conditioning phase, indicating that VR-based training could better engage the neural pathways responsible for MI. These findings align with previous research demonstrating the value of virtual environments in MA paradigms, whether for motor training with an XVA controlled through gaze direction and diaphragmatic modulation [4], or for MI of an extra thumb [9]. Notably, our study begins to bridge the gap between these two approaches by exploring the use of neural correlates during the imagined movement of an entire extra limb, rather than a single finger. It serves as a proof-of-concept baseline, demonstrating that such neural modulation occurs even without prior XVA MI training.

Finally, while identifying the specific brain regions involved in the MI of an XVA is an important and compelling question, the present study did not aim to localize cortical sources due to the intrinsic limitations of EEG in spatial resolution. Neural recordings via EEG are well-suited for capturing the temporal and spectral characteristics of motor-related activity, for example, but do not allow for reliable inference about the involvement of specific cortical areas.

It is worth noting that the observed effect sizes across the arm conditions were generally small. This may reflect the nature of the neural modulation involved in the motor imagery of both biological and virtual limbs. Rather than exhibiting strong, localized desynchronization patterns over classic contralateral motor areas, the effects appeared to be more spatially diffuse, engaging broader regions of the sensorimotor cortex. Such distributed activation is consistent with previous findings in motor imagery of whole-limb movements or unfamiliar effectors, where the neural representation is less focal and may require wider cortical recruitment for planning and control [32], [33]. This pattern is especially plausible in the context of a novel effector like the XVA, where participants likely engage compensatory or associative regions to simulate motor control in the absence of a well-established somatotopic representation.

The asymmetry observed between left and right arm MI in our ERD/S analysis (Fig. 3F–G) deserves some further interpretation. Although symmetrical neural modulation would be expected in ideal conditions, MI is inherently variable, particularly in the absence of real movement or external feedback. Participants may differ in how vividly or consistently they imagine actions with each limb. Importantly, these results were not derived from single or contralateral electrodes but rather from a central ROI encompassing all frontocentral, central, and centroparietal channels. Therefore, the differences do not reflect electrode selection bias, but rather true variability in group-level neural responses to motor imagery across limbs.

A full understanding of the neural substrates supporting XVA control likely depends on multiple factors, including the novelty of the effector, its spatial location on the body (e.g., midline vs. lateral), the cognitive strategy used during MI, and the duration or specificity of training. Additionally, we anticipate that active control of the extra limb, beyond passive observation or imagery, would further modulate its neural representation, potentially leading to stronger, more localized, and more consistent activation patterns. These aspects, although not the primary focus of our current study, are critical to understand how the brain allocates resources to control non-biological limbs. Future research combining MI and active control paradigms with neuroimaging techniques that offer higher spatial resolution (e.g., source-localized EEG, MEG, or fMRI) will be essential to more precisely characterize the cortical networks underlying the representation and integration of supernumerary limbs.

B. Classification of MI Neural Patterns

Our findings demonstrate not only the ability to detect neural signatures associated with MI but also to classify them with reasonable accuracy. Using a Riemannian-based decoding approach, we achieved significant classification accuracy for the three arms (left, right, and XVA) in the Pre condition, consistently exceeding chance levels. Interestingly, the XVA was consistently the most accurately decoded across all cases. We speculate that this may be due to a combination of heightened concentration and focus during the XVA trials, driven by their novelty, along with a potentially distinct underlying neural activity pattern that characterizes this MI compared to that of biological limbs. However, it is also important to highlight the lateralization effect observed in decoding performance when the right-side channels were removed (Fig. 5). This suggests that neural modulation and encoding associated with the MI process might be primarily represented in this region. Furthermore, the absolute changes in predictions shown in the median confusion matrices in

Fig. 5C indicate that the decoding of XVA trials was also influenced by lateralization, suggesting that the observed effects were not limited to the classification of Right and Left arm trials. One possible explanation is that while Right Arm MI and XVA MI primarily engage similar neural processes in the left hemisphere, as suggested by Figs. 2 and 3F–G and discussed in Section IV-A, the XVA condition also presents additional right hemisphere modulation. Consequently, when only left-side channels remain, the neural activity patterns of these two classes may become harder to distinguish, resulting in reduced classification accuracy. This interpretation is further supported by the observation that, in Fig. 5C, the changes in misclassifications due to lateralization involved only Right Arm and XVA trials. It remains to be determined whether this is a general phenomenon or if the observed overlap in representation between the XVA and the real arm is influenced by the right-handedness of our participants. If that is the case, it could be speculated that participants naturally imagine the movement of the XVA similarly to their dominant arm. However, it would be interesting to investigate in future studies if, with appropriate training, the neural representation would change and become more distinct.

The advantage of the Riemannian classifier lies in its ability to leverage the intrinsic neural representation of movements by operating on covariance matrices [20], [21]. This approach highlights distinct neural patterns across channels, which may contribute to its effectiveness in decoding different movement intentions. However, we observed a decrease in decoding performance in the Post phase for both the T and NT groups, despite the neural correlates appearing stronger after conditioning. We hypothesize that this decline may be attributed to the classification algorithm itself, which does not rely on explicitly engineered features and primarily analyzes signals in the temporal domain rather than specific frequency bands. While some neural correlates may have strengthened, the overall covariance patterns might have remained stable or become more ambiguous, potentially affecting decoding accuracy. This effect was particularly pronounced in the T group, where decoding accuracy in the Post phase did not reach significance. One possible explanation is that tactile feedback introduced a disruptive element, reducing participants' attentional focus. This interpretation is further supported by the illustration of the XVA covariance centroids, which revealed greater stability in the NT group compared to the T group between the Pre and Post phases.

Additionally, our temporal analysis highlighted distinct neural engagement for XVA imagery. It is important to note that decoding accuracies in the time-resolved analysis in Fig. 6A were slightly lower than those computed when using the whole trials. This is likely due to the computation of covariance matrices within 500 ms time windows rather than over the full 5-second MI period. Interestingly, no apparent decrease in performance was observed for the NT group in this analysis. Furthermore, examining the NT group's decoding accuracy profiles revealed a shift in temporal dynamics. In the Pre phase, a single peak emerged around 1 second after the Go signal. However, in the Post phase, a more sustained decoding accuracy was observed from 1 s to 3.4 s after the Go signal, with two distinct peaks. This suggests that the conditioning phase may have enhanced the imagery process, making it more persistent over time.

Although the XVA consistently exhibited weaker ERD amplitude compared to the biological limbs (Fig. 2F–G), it yielded the highest decoding accuracy across conditions. This apparent discrepancy can be explained by the spatial properties of the neural signals and the decoding method employed. The Riemannian classifier relies on spatial covariance matrices, which encode inter-channel dependencies rather than isolated power levels. In this context, the XVA's more distributed and scattered representation, revealed in our lateralization analysis, may produce a more unique and distinguishable spatial signature, even if the overall amplitude of desynchronization is lower. Unlike biological arms, which may activate more stereotyped and lateralized regions, the XVA's representation likely engages a more variable set of sensorimotor channels, leading to a distinct covariance structure that the classifier can reliably detect. These results highlight the importance of considering spatial encoding, not just amplitude, when interpreting decoding performance based on MI.

Interestingly, the analysis designed to better approximate a pseudo-online scenario (Fig. 6B) yielded comparable results: significant classification accuracies were observed for both the T and NT groups in the Pre condition, but only for the NT group in the Post condition. Additionally, the temporal profiles in Fig. 6B appear smoother than those in Fig. 6A. This likely reflects the greater stability of a single classifier trained on covariance matrices derived from longer time windows, as opposed to models trained on shorter segments. Overall, these findings underscore the translational potential of our approach and support its applicability in real-time BMI settings for controlling the XVA.

Our decoding analysis focused exclusively on the three classes corresponding to the arms involved in the MI process, without including a "rest" class. While this design choice represents a limitation and raises questions about the potential decoding of the XVA class against the "rest" class, it is important to emphasize the clear neural modulation observed during the MI of the XVA compared to the preparation period. This shows the presence of distinct neural patterns separate from baseline activity. Nonetheless, we acknowledge that incorporating the "rest" class will be a critical step in future developments of BMIs to enable effective control of external devices, for instance, by allowing the rest state to serve as a signal to halt ongoing movements.

C. The Role of Tactile Feedback in the Conditioning Phase

In this study, we sought to incorporate a sensory dimension into MI to further investigate the neural correlates of controlling an XVA. Specifically, we introduced tactile feedback during the conditioning phase in VR to strengthen the sensory input associated with the XVA's movement. Literature highlights the potential of kinesthetic motor imagery—which emphasizes the sensation of movement rather than its visual representation—to enhance MI processes. Kinesthetic MI has been shown to engage sensorimotor networks more

robustly, fostering a stronger connection between imagined and executed actions [34], [35]. However, incorporating sensory feedback for extra limbs presents a unique challenge, as subjects do not inherently possess an established sensory representation for such novel appendages [1].

To address this, we integrated tactile feedback to help subjects associate a physical sensation with XVA movement. Surprisingly, our findings reveal that the impact of tactile feedback on neural engagement was less significant than anticipated. One possible explanation lies in the simplicity of the task, which involved only forward and backward arm movements [4]. This straightforward motion may not have been complex enough to capitalize on the potential benefits of tactile feedback or the sensory encoding strategies could be further explored. In such scenarios, visual feedback likely dominated, aligning directly with the motor intention of the XVA. While kinesthetic MI is generally expected to outperform visual MI in engaging sensorimotor regions [33], its effectiveness is often influenced by the subject's prior experience. Evidence suggests that individuals with more experience in kinesthetic MI tasks exhibit greater neural engagement [36]. Without prior familiarity or robust sensory association, the tactile feedback may have introduced sensory confusion, as it was exclusively linked to the XVA and not the biological arms. Additionally, the inherent dominance of visual inputs [37], particularly in MA contexts, may have further reduced the contribution of tactile feedback.

We hypothesize that more complex movements, such as those involving multi-joint coordination or varied gestures or object interactions, could better leverage tactile feedback by enhancing the perception of the XVA's movement and facilitating its integration with the MI process. Other sensory modalities, encoding strategies, extended habituation, and training might also be other factors that can strengthen this sensory association, improving neural engagement over time, and are worth further investigation.

Another potential factor could be the conditioning process itself. The tactile feedback was introduced passively, which may have been insufficient to establish a strong neural link between the sensation and motor control of the XVA. As the XVA represents an unconventional "tool" rather than a biological limb, the association between tactile input and movement may require longer, more dynamic, and interactive conditioning paradigms.

V. Conclusion

Exploring the role of MI in the context of extra limbs presents not only a solution to control xDoFs in MA paradigms, but also a unique opportunity to innovate BMI solutions further. Our findings highlight the adaptability of the brain's motor systems in accommodating novel appendages, as evidenced by similar yet distinguishable neural signatures of MI of biological arms and the XVA. Even though maximizing decoding accuracy was not the focus of the present study, we showed the feasibility of classifying XVA-related MI patterns, which represents a crucial step towards the development of BMI for MA. In addition, VR-based conditioning effectively enhanced neural engagement during MI tasks, particularly in the α and β rhythms, suggesting its value for training protocols. However, we found that tactile feedback introduced during the conditioning phase yielded less pronounced effects than expected, potentially due to the task's simplicity, to the dominance of visual inputs, and to the novelty linked to the association of tactile sensations with an unconventional tool such as the XVA. Future studies should investigate alternative encoding strategies and sensory modalities to better understand the role of feedback in controlling extra limbs. Additionally, exploring new or complementary decoding algorithms, alongside more refined preprocessing pipelines and feature extraction techniques, will be essential for enhancing classification accuracy and adapting this approach for real-time applications. These findings collectively highlight the potential of MI in MA, both for directly controlling xDOFs and for enhancing the training process through neural engagement, similar to its applications in rehabilitation contexts.

Acknowledgment

The authors thank all the participants in this study together with Tobias Bodenmann, Thibaut Stoltz, Elena Gado, and Marwan Haioun for their help in the data acquisition. Solaiman Shokur and Silvestro Micera are equally contributed senior authors.

Daniel Leal Pinheiro is with the Translational Neural Engineering Lab, Neuro-X Institute, Ecole Polytechnique Federale de Lausanne, 1202 Geneve, Switzerland, and also with the Translational Neural Engineering Lab, The BioRobotics Institute, Health Interdisciplinary Center and Department of Excellence in Robotics and AI, Scuola Superiore Sant'Anna, 56127 Pisa, Italy.

Leonardo Pollina is with the Translational Neural Engineering Lab, Neuro-X Institute, Ecole Polytechnique Federale de Lausanne, 1202 Geneve, Switzerland.

Karin A. Buetler is with the Motor Learning and Neurorehabilitation Laboratory, ARTORG Center for Biomedical Engineering Research, University of Bern, 3012 Bern, Switzerland.

Laura Marchal-Crespo is with the Department of Rehabilitation Medicine, Erasmus Medical Center, 3015 GD Rotterdam, The Netherlands, and also with the Department of Cognitive Robotics, TU Delft, 2628 Delft, The Netherlands.

Solaiman Shokur is with the Translational Neural Engineering Lab, Neuro-X Institute, Ecole Polytechnique Federale de Lausanne, 1202 Geneve, Switzerland, also with the Modular Implantable Neurotechnologies Lab, Università Vita-Salute San Raffaele, 20132 Milan, Italy, also with the Sensorimotor Neurotechnology Lab, The BioRobotics Institute, Health Interdisciplinary Center and Department of Excellence in Robotics and AI, Scuola Superiore Sant'Anna, 56127 Pisa, Italy, and also with the Department of Clinical Neurosciences, University Hospital of Lausanne, University of Lausanne, 1015 Lausanne, Switzerland.

Silvestro Micera is with the Translational Neural Engineering Lab, Neuro-X Institute, Ecole Polytechnique Federale de Lausanne, 1202 Geneve, Switzerland, also with the Translational Neural Engineering Lab, The BioRobotics Institute, Health Interdisciplinary Center and Department of Excellence in Robotics and AI, Scuola Superiore Sant'Anna, 56127 Pisa, Italy, and also with the Modular Implantable Neurotechnologies Lab, Università Vita-Salute San Raffaele, 20132 Milan, Italy (e-mail: silvestro.micera@epfl.ch).

References

[1] G. Dominijanni et al., "The neural resource allocation problem when enhancing human bodies with extra robotic limbs," *Nat. Mach. Intell.*, vol. 3, no. 10, pp. 850–860, Oct. 2021. [Online]. Available: https://www.nature.com/articles/s42256-021-00398-9

[2] D. Prattichizzo et al., "Human augmentation by wearable supernumerary robotic limbs: Review and perspectives," *Prog. Biomed. Eng.*, vol. 3, no. 4, Sep. 2021, Art. no. 42005. [Online]. Available: https://dx.doi.org/10.1088/2516-1091/ac2294

[3] J. Eden et al., "Principles of human movement augmentation and the challenges in making it a reality," *Nat. Commun.*, vol. 13, no. 1, p. 1345, Mar. 2022. [Online]. Available: https://www.nature.com/articles/s41467-022-28725-7

[4] G. Dominijanni et al., "Human motor augmentation with an extra robotic arm without functional interference," *Sci. Robot.*, vol. 8, no. 85, Dec. 2023, Art. no. eadh1438. [Online]. Available: https://www.science.org/doi/10.1126/scirobotics.adh1438

[5] P. Kieliba, D. Clode, R. O. Maimon-Mor, and T. R. Makin, "Robotic hand augmentation drives changes in neural body representation," *Sci. Robot.*, vol. 6, no. 54, May 2021, Art. no. eabd7935.

[6] D. Leal Pinheiro, G. Dominijanni, F. P. Maenza, H. Dirat, S. Shokur, and S. Micera, "Exploring skill generalization with an extra robotic arm for motor augmentation," *Adv. Intell. Syst.*, to be published.

[7] M. Bräcklein, J. Ibáñez, D. Y. Barsakcioglu, and D. Farina, "Towards human motor augmentation by voluntary decoupling beta activity in the neural drive to muscle and force production," *J. Neural Eng.*, vol. 18, no. 1, Feb. 2021, Art. no. 16001.

[8] D. J. L. L. Pinheiro, J. Faber, S. Micera, and S. Shokur, "Human-machine interface for two-dimensional steering control with the auricular muscles," *Front. Neurorobot.*, vol. 17, Jun. 2023, Art. no. 1154427. [Online]. Available: https://www.frontiersin.org/journals/neurorobotics/articles/10.3389/fnbot.2023.1154427/full

[9] H. Alsuradi et al., "Neural signatures of motor imagery for a supernumerary thumb in VR: An EEG analysis," *Sci. Rep.*, vol. 14, no. 1, Sep. 2024, Art. no. 21558. [Online]. Available: https://www.nature.com/articles/s41598-024-72358-3

[10] M. Lotze and U. Halsband, "Motor imagery," *J. Physiol. Paris*, vol. 99, nos. 4–6, pp. 386–395, Jun. 2006.

[11] J. Munzert, B. Lorey, and K. Zentgraf, "Cognitive motor processes: The role of motor imagery in the study of motor representations," *Brain Res. Rev.*, vol. 60, no. 2, pp. 306–326, May 2009.

[12] G. Buccino et al., "Action observation activates premotor and parietal areas in a somatotopic manner: An fMRI study," *Eur. J. Neurosci.*, vol. 13, no. 2, pp. 400–404, Jan. 2001.

[13] G. Pfurtscheller and F. H. Lopes da Silva, "Event-related EEG/MEG synchronization and desynchronization: Basic principles," *Clin. Neurophysiol.*, vol. 110, no. 11, pp. 1842–1857, Nov. 1999.

[14] K. Nakayashiki, M. Saeki, Y. Takata, Y. Hayashi, and T. Kondo, "Modulation of event-related desynchronization during kinematic and kinetic hand movements," *J. NeuroEng. Rehabil.*, vol. 11, no. 1, p. 90, May 2014. [Online]. Available: https://doi.org/10.1186/1743-0003-11-90

[15] Y.-H. Liu, L.-F. Lin, C.-W. Chou, Y. Chang, Y.-T. Hsiao, and W.-C. Hsu, "Analysis of electroencephalography event-related desynchronisation and synchronisation induced by lower-limb stepping motor imagery," *J. Med. Biol. Eng.*, vol. 39, no. 1, pp. 54–69, Feb. 2019. [Online]. Available: https://doi.org/10.1007/s40846-018-0379-9

[16] B. H. Dobkin, "Brain-computer interface technology as a tool to augment plasticity and outcomes for neurological rehabilitation," *J. Physiol.* vol. 579, pp. 637–642, Mar. 2007.

[17] P. D. Marasco, K. Kim, J. E. Colgate, M. A. Peshkin, and T. A. Kuiken, "Robotic touch shifts perception of embodiment to a prosthesis in targeted reinnervation amputees," *Brain*, vol. 134, no. 3, pp. 747–758, 2011.

[18] A. M. Ladda, F. Lebon, and M. Lotze, "Using motor imagery practice for improving motor performance—A review," *Brain Cogn.*, vol. 150, Jun. 2021, Art. no. 105705.

[19] G. Pfurtscheller and C. Neuper, "Motor imagery activates primary sensorimotor area in humans," *Neurosci. Lett.*, vol. 239, nos. 2–3, pp. 65–68, Dec. 1997.

[20] A. Barachant, S. Bonnet, M. Congedo, and C. Jutten, "Classification of covariance matrices using a Riemannian-based kernel for BCI applications," *Neurocomputing*, vol. 112, pp. 172–178, Jul. 2013. [Online]. Available: https://www.sciencedirect.com/science/article/pii/S0925231213001574

[21] M. Congedo, A. Barachant, and R. Bhatia, "Riemannian geometry for EEG-based brain-computer interfaces; a primer and a review," *Brain-Comput. Interfaces*, vol. 4, no. 3, pp. 155–174, Jul. 2017, doi: 10.1080/2326263X.2017.1297192.

[22] M. C. Ottenhoff et al., "Decoding executed and imagined grasping movements from distributed non-motor brain areas using a Riemannian decoder," *Front. Neurosci.*, vol. 17, Nov. 2023, Art. no. 1283491. [Online]. Available: https://www.frontiersin.org/journals/neuroscience/articles/10.3389/fnins.2023.1283491/full

[23] A. Barachant et al. "Pyriemann." Feb. 2025. [Online]. Available: https://doi.org/10.5281/zenodo.593816

[24] S. Kumar, H. Alawieh, F. S. Racz, R. Fakhreddine, and J. D. R. Millán, "Transfer learning promotes acquisition of individual BCI skills," *PNAS Nexus*, vol. 3, no. 2, 2024, Art. no. pgae076. [Online]. Available: https://doi.org/10.1093/pnasnexus/pgae076

[25] K. Mitra, F. S. Racz, S. Kumar, A. D. Deshpande, and J. Del R. Millán, "Characterizing the onset and offset of motor imagery during passive arm movements induced by an upper-body exoskeleton," in *Proc. IEEE/RSJ Int. Conf. Intell. Robots Syst. (IROS)*, 2023, pp. 3789–3794. [Online]. Available: https://ieeexplore.ieee.org/document/10342492

[26] G. Pfurtscheller, A. Stancak Jr., and C. Neuper, "Post-movement beta synchronization. A correlate of an idling motor area?" *Electroencephalogr. Clin. Neurophysiol.*, vol. 98, no. 4, pp. 281–293, 1996.

[27] C. Neuper and G. Pfurtscheller, "Event-related dynamics of cortical rhythms: Frequency-specific features and functional correlates," *Int. J. Psychophysiol.*, vol. 43, no. 1, pp. 41–58, 2001.

[28] G. Pfurtscheller, C. Neuper, C. Brunner, and F. L. Da Silva, "Beta rebound after different types of motor imagery in man," *Neurosci. Lett.*, vol. 378, no. 3, pp. 156–159, 2005.

[29] T. Mulder, "Motor imagery and action observation: Cognitive tools for rehabilitation," *J. Neural Transm.*, vol. 114, no. 10, pp. 1265–1278, Oct. 2007. [Online]. Available: https://www.ncbi.nlm.nih.gov/pmc/articles/PMC2797860/

[30] D. L. Eaves, M. Riach, P. S. Holmes, and D. J. Wright, "Motor imagery during action observation: A brief review of evidence, theory and future research opportunities," *Front Neurosci.*, vol. 10, p. 514, Nov. 2016.

[31] D. L. Eaves, N. J. Hodges, G. Buckingham, G. Buccino, and S. Vogt, "Enhancing motor imagery practice using synchronous action observation," *Psychol. Res.*, vol. 88, no. 6, pp. 1891–1907, 2024.

[32] A. J. Szameitat, S. Shen, and A. Sterr, "Motor imagery of complex everyday movements. An fMRI study," *Neuroimage*, vol. 34, no. 2, pp. 702–713, 2007.

[33] C. Neuper, R. Scherer, M. Reiner, and G. Pfurtscheller, "Imagery of motor actions: Differential effects of kinesthetic and visual-motor mode of imagery in single-trial EEG," *Brain Res. Cogn. Brain Res.*, vol. 25, no. 3, pp. 668–677, Dec. 2005.

[34] A. Orlandi, E. Arno, and A. M. Proverbio, "The effect of expertise on kinesthetic motor imagery of complex actions," *Brain Topogr.*, vol. 33, no. 2, pp. 238–254, Mar. 2020.

[35] Y. J. Yang, E. J. Jeon, J. S. Kim, and C. K. Chung, "Characterization of kinesthetic motor imagery compared with visual motor imageries," *Sci. Rep.*, vol. 11, no. 1, p. 3751, Feb. 2021.

[36] K. R. Ridderinkhof and M. Brass, "How kinesthetic motor imagery works: A predictive-processing theory of visualization in sports and motor expertise," *J. Physiol. Paris*, vol. 109, nos. 1–3, pp. 53–63, 2015.

[37] J. Hartcher-O'Brien, C. Levitan, and C. Spence, "Extending visual dominance over touch for input off the body," *Brain Res.*, vol. 1362, pp. 48–55, Nov. 2010.